Soft Matter

COMMUNICATION

View Article Online
View Journal | View Issue

Cite this: *Soft Matter*, 2016, 12, 2663

Received 19th December 2015,
Accepted 10th February 2016

DOI: 10.1039/c5sm03068d

www.rsc.org/softmatter

Assembly of nothing: equilibrium fluids with designed structured porosity†

Beth A. Lindquist, Ryan B. Jadrich and Thomas M. Truskett*

Controlled micro- to meso-scale porosity is a common materials design goal with possible applications ranging from molecular gas adsorption to particle size selective permeability or solubility. Here, we use inverse methods of statistical mechanics to design an isotropic pair interaction that, in the absence of an external field, assembles particles into an inhomogeneous fluid matrix surrounding pores of prescribed size ordered in a lattice morphology. The pore size can be tuned *via* modification of temperature or particle concentration. Moreover, modulating density reveals a rich series of microphase-separated morphologies including pore- or particle-based lattices, pore- or particle-based columns, and bicontinuous or lamellar structures. Sensitivity of pore assembly to the form of the designed interaction potential is explored.

Synthesis of materials with controlled micro- to meso-scale porosity is a design challenge ripe for new, innovative approaches. For example, ordered porous zeolite solids – commonplace for their use as molecular sponges to absorb gases – have recently inspired an extension to the liquid state *via* molecular cages dispersed in a solvent of larger excluded molecules to form an absorbing "pore fluid".[1] At the colloidal level, control over the effective particle interactions can lead to equilibrium structures with large percolating voids (*i.e.*, connected regions of solvent-occupied, but particle-free, space), as was recently highlighted *via* a computational study of indented particles with depletion attractions.[2] Prior theoretical work[3–6] suggests that even a single-component system interacting *via* an isotropic pair potential comprising competitive attractive and repulsive components can form an equilibrium fluid with a porous structure. Such systems also appear to have modified vapor-liquid phase behavior leading to coexistence involving modulated phases.[6] Even a simple two-dimensional lattice model with competing interactions was shown to assemble into a fluid phase with "bubbles" or pores, among other microphases;[7] a two-dimensional continuum theory yields similar predictions.[8] Such results are reminiscent of experimentally observed interfacial structures of colloids with competing interactions.[9] Here, we explore the prospect of using inverse methods of statistical mechanics to discover which (if any) isotropic pairwise interactions spontaneously assemble particles into an inhomogeneous three-dimensional fluid matrix surrounding ordered, monodisperse spherical pores of prescribed size. We further study how the microphase structure of such a model material would respond to changes in temperature and particle concentration or depend on the specific form of the interaction. The ability to control the size and spatial organization of pore structures in fluids, *via* interactions and thermodynamic parameters, could help pave the way for novel colloidally assembled structures with programmable particle-size-selective permeability/solubility similar to materials templated *via* block-copolymer assembly[10] (with selective etching of one block component to create void space).

Modern computational coarse-graining[11,12] and inverse design strategies are ideally suited for the optimization of pair interactions to realize complex, self-assembled material architectures. Previously, inverse design has led to the discovery of isotropic, convex-repulsive pair interactions that stabilize exotic, open crystalline arrangements (*e.g.*, honeycomb and diamond lattices).[13,14] Another example is the design of pair interactions that promote the formation of a fluid of well-defined equilibrium particle clusters (*i.e.*, microscopic liquid droplets).[15] Here, we use iterative Boltzmann inversion (IBI)[11,15] to find the dimensionless, isotropic pair potential $\beta u_{\mathrm{IBI}}(r)$ [where $\beta = (k_{\mathrm{B}}T)^{-1}$, k_{B} is the Boltzmann constant, and T is temperature] which best reproduces, at equilibrium, the radial distribution function (RDF), $g_{\mathrm{tgt}}(r)$, of our target structure: a fluid matrix of particles surrounding a lattice of pores or voids with prescribed size.

The configurational ensemble of the target structure is generated from a molecular simulation of an inhomogeneous fluid of effective hard-core Weeks–Chandler–Andersen (WCA) particles of diameter σ embedded in the interstitial space of a lattice of larger WCA particles of diameter 4σ; the latter enforces the ordered pore structure by excluding the target

McKetta Department of Chemical Engineering, University of Texas at Austin, Austin, TX 78712, USA. E-mail: truskett@che.utexas.edu

† Electronic supplementary information (ESI) available: Computational methods, cluster size distributions, and analytical form and optimized parameters from relative entropy optimizations. See DOI: 10.1039/c5sm03068d

fluid particles. The large particles were fixed on an FCC lattice with a nearest-neighbor distance of 7.4σ. This choice was motivated to balance two competing effects: (1) to maximize the pore signature in $g_{tgt}(r)$ while (2) furnishing pore "walls" formed by the fluid matrix with a thickness comparable to the pore size (*i.e.*, a pore center-to-center distance of approximately two times the pore diameter). The latter consideration was inspired by preliminary optimizations for several target simulations, which showed that the potential developed a repulsive hump centered near the pore size (irrespective of whether that potential successfully formed pores). This occurs so that a particle bordering a pore will impede other particles from entering the pore on the opposite side, as shown on the leftmost pore in the scheme in Fig. 1a, where the repulsive hump for a selected particle is highlighted in green and the schematic is appropriately scaled. A system where the pore wall width and pore diameter are matched is optimal for description with a pair potential so that the highlighted particle can also contribute to the repulsive barrier at the edge of an adjacent pore, as shown for the rightmost pore in Fig. 1a. Additional details regarding the construction of the target system, including the effect of varying the large particle template, can be found in the Computational Methods section of the ESI.†

The IBI-optimized pair potential $\beta u_{IBI}(r)$ is shown in Fig. 1b. Even though there may be non-trivial many-body effects in an actual pore-forming system that are not captured by this strategy, an understanding of an isotropic pair potential that forms pores is useful because it (1) guarantees that many-body potentials exist that will also generate pores, and (2) reveals what those many-body interactions must map onto if they are projected into a pair interaction form. From prior work on microphase-separated states, it is not surprising that $\beta u_{IBI}(r)$ possesses competitive attractions and repulsions. The general form of the potential is similar in spirit to the cluster fluid-forming potentials that we reported in previous work,[15] though here the attractive well is generally narrower and deeper and the repulsive hump is broader but shorter when compared to clusters of similar size to the pores studied here. Common to both potentials is that the relevant lengthscales of the microphase-separated objects are directly encoded by the potential: for clusters, the position of the repulsive hump was directly related to cluster size, and here the repulsive hump is maximal at the prescribed pore size.

Also similarly to our previous cluster work, we observed good convergence in the IBI scheme. As can be seen in Fig. 1c, $\beta u_{IBI}(r)$ is indeed able to closely reproduce the equilibrium RDF of the inhomogeneous, target matrix of fluid particles at a packing fraction, $\eta = \pi\sigma^3 N/6V = 0.31$ where N is the number of particles and V is the volume. For comparison, the RDF of an isotropic, single-component WCA fluid with the same isothermal compressibility ($\eta = 0.42$) is also shown. Interestingly, the RDF of a dense fluid matrix surrounding pores (whether from the target or IBI model structure) is only subtly different from that of the equi-compressible isotropic WCA fluid, with the former being distinguished from the latter by its relatively suppressed correlations on the scale of the pore size, as highlighted in the inset. However, despite its success at reproducing the pair correlations

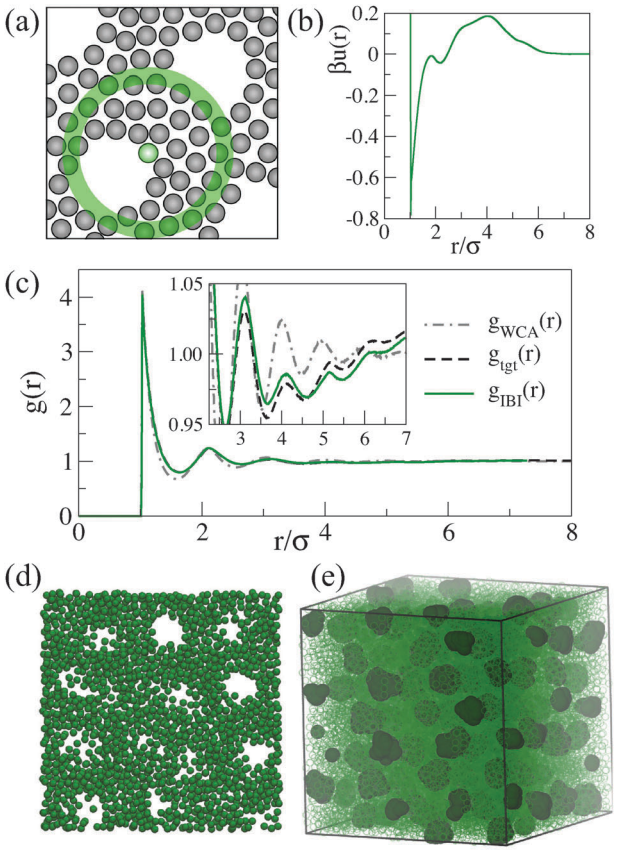

Fig. 1 Design of a pair potential, $\beta u_{IBI}(r)$, that assembles particles into a fluid matrix surrounding a lattice of pores. (a) Schematic for a system with matching pore diameter and pore wall thickness, where the repulsive hump in $\beta u_{IBI}(r)$ is shown in green for the highlighted particle. (b) The optimized pair potential, $\beta u_{IBI}(r)$. (c) Radial distribution functions for the targeted configurational ensemble of the fluid matrix particles ($\eta = 0.31$), a system of particles with the IBI-optimized pair potential ($\eta = 0.31$), and an isotropic, single-component WCA fluid with the same isothermal compressibility ($\eta = 0.42$). (inset) Zoomed view of main frame. (d) Image of a 3σ thick slab extracted from an equilibrium simulation configuration of particles with the IBI-optimized pair potential, illustrating pores. (e) Dark green regions show a three-dimensional visualization of the assembled BCC pore structure and represent the union volume of all 2σ diameter test spheres that could be successfully accommodated into the configuration without overlapping lighter green fluid particles interacting *via* the IBI-optimized pair potential.

of the target structure, it is not obvious that a system of particles interacting *via* $\beta u_{IBI}(r)$ will also necessarily capture the desired pore structure of the target ensemble, which depends on many-particle static correlations.

Nonetheless, we do find that pore structures very similar to those templated by the ordered lattice of large WCA spheres of the target system emerge with the IBI-optimized interaction, $\beta u_{IBI}(r)$. Hints of the pore morphology can be seen in Fig. 1d from a visual representation of the particles within a 3σ thick slab obtained from an equilibrium configuration. However, for a more quantitative characterization, 'pores' defined *via* a clustering analysis[16] as union volumes of all 2σ diameter test spheres that could be successfully accommodated into the configuration without overlapping the fluid matrix particles

were also examined. As described in ESI,† the size of an individual pore in a configuration is computed from its volume, obtained by Monte Carlo integration of overlapping inserted test particles, and is reported here as the diameter d_{eff} of an equivolume spherical pore. Fig. 1e shows that the pores (compact, dark green entities embedded in the lighter green matrix of fluid particles) actually form a BCC lattice with a lattice constant of 8.8σ (*i.e.*, nearest neighbor distance of 7.6σ). As can be seen from the solid green line in Fig. 2, the most likely effective diameter (d_{eff}) of an individual pore is 3.97σ, very close to desired 4σ pore size of the target ensemble. In other words, the IBI pair potential optimized to precisely match the RDF of the target ensemble also faithfully reproduces the ordered pore morphology of the target structure.

We next evaluate the sensitivity of the pore morphology of the system with the IBI-optimized pair potential to rescaling the temperature by a factor λ as $T \rightarrow \lambda T$ [equivalent to rescaling $\beta u_{\mathrm{IBI}}(r) \rightarrow \beta u_{\mathrm{IBI}}(r)/\lambda$]. Fig. 2 shows the pore size distribution function for equilibrium simulations with both mild cooling ($\lambda = 0.9$) and heating ($\lambda = 1.05$). With increasing temperature, we note the pores monotonically shrink and have larger size fluctuations, with no evident porosity accessible to the 2σ test particles by $\lambda = 1.1$. The inset in Fig. 2 shows that the total volume of the simulation box taken up by the pores correspondingly decreases with increasing temperature. The opposite trends occur with cooling – pores grow and become more uniform in size – until eventually the pores condense into "columns" of void space (by $\lambda = 0.8$). Nonetheless, bracketed by these two extremes, there is a range of temperature where approximately spherical pores form in a BCC lattice, and their size can be tuned *via* modification of the temperature.

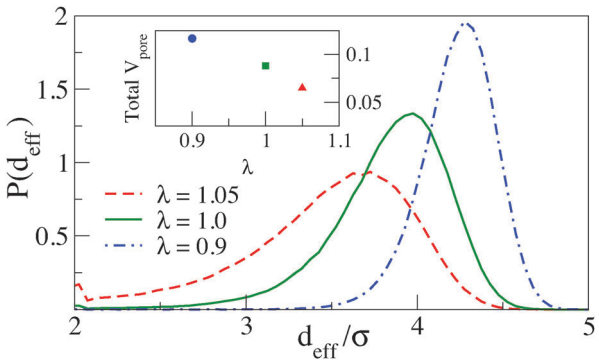

Fig. 2 Pore size probability distribution function $P(d_{\mathrm{eff}})$ for different choices of the temperature rescale parameter λ corresponding to the change $T \rightarrow \lambda T$ or equivalently $\beta u_{\mathrm{IBI}}(r) \rightarrow \beta u_{\mathrm{IBI}}(r)/\lambda$. (inset) Total volume of the pores as a function of λ.

Although small changes in packing fraction (η) also allow for tuning the pore size, we find that larger changes in η give rise to a rich diagram of microphase-separated void-particle morphologies. Fig. 3 shows configuration snapshots of the various microphases associated with $\beta u_{\mathrm{IBI}}(r)$ (highlighting particle and void structures, respectively) along with the corresponding density range for each phase. Densities of intermediate character are assigned to the phase that they most greatly resemble, with some buckling and/or defects present away from the optimal density for each phase. Upon reducing particle concentration from the optimized pore lattice structure, the pores first coalesce into void columns. Eventually the porous columns give way to a bicontinuous phase, where the void space and particles are interpenetrating. This gyroid-like phase then flattens out into lamellar sheets of alternating particles and voids. Lamellar sheets have been predicted for a single-component model with competing attractions and repulsions that also displays clustering behavior, but the possibility of pore lattices was not explored.[17] In two dimensions, an analogous striped phase has been observed in addition to a clustered phase for various models.[7]

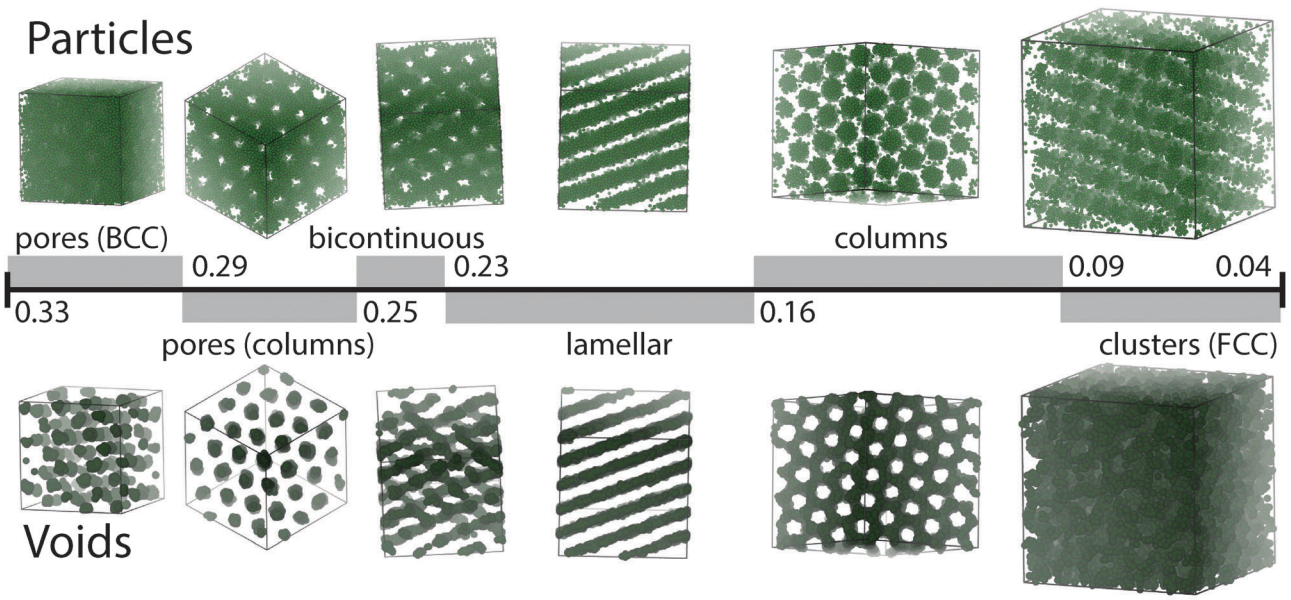

Fig. 3 Microphase diagram of the IBI-designed model as a function of η, with representative snapshots of each phase. Particles are depicted on the top row, and the inserted void particles are shown on the bottom row.

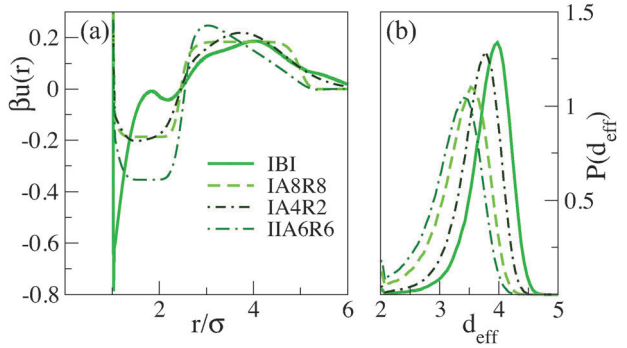

Fig. 4 Inverse designed pair potentials that form pores. (a) Potentials optimized with IBI and relative entropy approaches, where the latter are constrained to have a specific functional form (given in the ESI†). (b) Pore-size PDFs of the optimized potentials in (a).

The above phase progression of the void space has been seen in diblock copolymers as the relative amount of each block is tuned.[18] Here, η controls the ratio of void and particle-filled space. Upon further expansion from the lamellar phase, columns of particles are then formed, followed by clusters of particles as shown on the right hand side of Fig. 3. The particle clusters form with a preferred size, with radii of gyration ranging from $R_g = 2.00\sigma$ to 2.19σ as particle concentration is decreased; see the ESI.† The low-density region of the microphase diagram illustrates a symmetry between clusters and pores first postulated by Sear and Gelbart[3] and later predicted from theoretical calculations.[4,5] Intriguingly, microphases containing a single cluster and a single pore were observed from Grand Canonical Monte Carlo calculations of an SALR potential at different densities by Archer and Wilding.[6] This potential also showed a similar progression of phase behavior between these two state points, though the assembled structures had features on the order the size of the simulation box such that only a single column or sheet could form. As a result, it is unclear to what extent finite size effects impacted the characteristics of these phases. Here, we circumvent this difficulty by leveraging inverse design to systematically imbue a prescribed length scale to the features arising from microphase separation.

Finally, we explored the sensitivity of pore formation to the details of the interactions. Specifically, we performed new optimizations of the target ensemble using the relative entropy approach,[11,12] restricting the designed pair potential to a variety of functional forms, all containing a single attractive well plus a longer-ranged repulsive hump controlled by four scalar parameters (two energies and two length scales). The analytic forms of the optimized potentials are given in the ESI.† Fig. 4a compares $\beta u_{\mathrm{IBI}}(r)$ to three such optimized potentials, and Fig. 4b shows the resulting pore-size PDFs. All potentials form pore lattices, albeit with somewhat reduced pore sizes relative to $\beta u_{\mathrm{IBI}}(r)$ – though, as we showed above, the pore size can also be modulated *via* temperature. See the ESI† for corresponding simulation snapshots, where the discrete character of the pores is visually evident.

The variation in the potentials indicates that there are many ways to balance attractions and repulsions in order to achieve a porous microphase separated state, though the repulsive hump tends to be centered near the targeted pore size. Generally, we find that longer-ranged attractions than are traditionally found in microphase-separated models are preferred for forming size-specific pores. Although it might be difficult to realize such effective interactions for micron-sized colloidal particles, it should be possible for nanoscale particles. As an example, potentials of mean force observed in simulations of ligand-coated, charge-stabilized gold nanoparticles display a similar qualitative form.[19] Moreover, in future work, a similar relative entropy approach could be used to limit the range of the attraction for application to colloids as well as to explore the range of parameters that can be employed in the target simulation to successfully make pores, particularly with respect to pore size and pore density.

In conclusion, we have used inverse design to discover a pair potential that assembles particles into a fluid matrix surrounding a lattice of pores with prescribed size, in addition to other complex fluid-pore microphases analogous to those seen in diblock copolymer systems (clusters, columns, lamellar sheets, and a bicontinuous phase). We have further demonstrated that the assembly of such microphases can be achieved *via* a variety of different interaction potentials displaying competitive attractive and repulsive interactions.

Acknowledgements

This work was partially supported by the National Science Foundation (1247945) and the Welch Foundation (F-1696). We acknowledge the Texas Advanced Computing Center (TACC) at The University of Texas at Austin for providing HPC resources.

References

1 N. Giri, M. G. Del Pópolo, G. Melaugh, R. L. Greenaway, K. Rätzke, T. Koschine, L. Pison, M. F. C. Gomes, A. I. Cooper and S. L. James, *Nature*, 2015, **527**, 216–220.
2 D. J. Ashton, R. L. Jack and N. B. Wilding, *Phys. Rev. Lett.*, 2015, **114**, 237801.
3 R. P. Sear and W. M. Gelbart, *J. Chem. Phys.*, 1999, **110**, 4582–4588.
4 A. Ciach, J. Pekalski and W. T. Gozdz, *Soft Matter*, 2013, **9**, 6301–6308.
5 H. Shin, G. M. Grason and C. D. Santangelo, *Soft Matter*, 2009, **5**, 3629–3638.
6 A. J. Archer and N. B. Wilding, *Phys. Rev. E: Stat., Nonlinear, Soft Matter Phys.*, 2007, **76**, 031501.
7 N. G. Almarza, J. Pekalski and A. Ciach, *J. Chem. Phys.*, 2014, **140**, 164708.
8 A. J. Archer, *Phys. Rev. E: Stat., Nonlinear, Soft Matter Phys.*, 2008, **78**, 031402.
9 J. Ruiz-Garca, R. Gámez-Corrales and B. I. Ivlev, *Phys. Rev. E: Stat., Nonlinear, Soft Matter Phys.*, 1998, **58**, 660–663.
10 E. A. Jackson and M. A. Hillmyer, *ACS Nano*, 2010, **4**, 3548–3553.
11 W. G. Noid, *J. Chem. Phys.*, 2013, **139**, 090901.

12 A. Chaimovich and M. S. Shell, *J. Chem. Phys.*, 2011, **134**, 094112.
13 E. Marcotte, F. H. Stillinger and S. Torquato, *Soft Matter*, 2011, **7**, 2332–2335.
14 A. Jain, J. R. Errington and T. M. Truskett, *Soft Matter*, 2013, **9**, 3866–3870.
15 R. B. Jadrich, J. A. Bollinger, B. A. Lindquist and T. M. Truskett, *Soft Matter*, 2015, 9342–9354.
16 P. D. Godfrin, N. E. Valadez-Perez, R. Castaneda-Priego, N. J. Wagner and Y. Liu, *Soft Matter*, 2014, **10**, 5061–5071.
17 T. Jiang and J. Wu, *Phys. Rev. E: Stat., Nonlinear, Soft Matter Phys.*, 2009, **80**, 021401.
18 Y. Mai and A. Eisenberg, *Chem. Soc. Rev.*, 2012, **41**, 5969–5985.
19 R. C. Van Lehn and A. Alexander-Katz, *Langmuir*, 2013, **29**, 8788–8798.